The statistical hadronization model approach to $\sqrt{s_{NN}} = 200$ GeV Au-Au collisions: p_T-spectra fits and global variable predictions

Dariusz Prorok*
Institute of Theoretical Physics, University of Wrocław,
Pl.Maksa Borna 9, 50-204 Wrocław, Poland
(Dated: November 27, 2006)

Three possible scenarios of the statistical hadronization model are reexamined with the use of the p_T spectra of the PHENIX and very low p_T PHOBOS measurements at $\sqrt{s_{NN}} = 200$ GeV. These scenarios are: (*a*) full chemical non-equilibrium, (*b*) strangeness chemical non-equilibrium and (*c*) chemical equilibrium. Fits to the spectra are done within the Cracow single-freeze-out model, which takes into account both the expansion and resonance decays. Predictions for spectra of ϕ, $K(892)^{*0}$ and π^0 are also given. The global variables like the transverse energy at midrapidity, the charged particle multiplicity at midrapidity and the total multiplicity of charged particles are evaluated and their predicted values agree qualitatively well with the experimental data. The thorough analysis within this model suggests that the chemical full non-equilibrium case is the least likely and both other cases are of the similar likelihood. It is also shown that if the full chemical non-equilibrium freeze-out took place it could manifest itself in the enhancement of the π^0-production at very low transverse momenta.

PACS numbers: 25.75.-q, 25.75.Dw, 24.10.Pa, 24.10.Jv

I. INTRODUCTION

Since the first run of the Relativistic Heavy Ion Collider (RHIC) the great amount of data on the hadron production from the hot and dense fireball created in a collision have been available. In this paper the application of the statistical hadronization model (SHM) to the description of the fireball bulk properties [1] is reexamined with the use of the p_T spectra measured by the PHENIX Collaboration at the top RHIC energy $\sqrt{s_{NN}} = 200$ GeV [2].

In the SHM the formation process of each particle is described on the basis of the assumption that the accessible phase space is fully saturated (maximized). Then the particle yields are determined by their phase space weight which is given by a statistical distribution (for a comprehensive review of the model see [3]). The main feature of this model is that it allows to deviate from the usually presumed chemical equilibrium of the fireball at the freeze-out. This has been achieved via the introduction of some new parameters, so-called phase-space occupancy factors: γ_q for light quarks and γ_s for strange quarks in hadrons. In Ref. [1] three possible cases were considered:

1. Full chemical non-equilibrium, $\gamma_q \neq 1$, $\gamma_s \neq 1$.
2. Strangeness chemical non-equilibrium (semi-equilibrium), $\gamma_q = 1$, $\gamma_s \neq 1$.
3. Chemical equilibrium, $\gamma_q = 1$, $\gamma_s = 1$.

The phase-space occupancy factors γ_q and γ_s together with the temperature T and baryon number chemical potential μ_B comprise the full set of independent statistical parameters of the model. For all three cases of chemical non-equilibrium/equilibrium, values of these parameters have been determined in Ref. [1]. This was done for each centrality bin of the PHENIX measurement at $\sqrt{s_{NN}} = 200$ GeV from fits to the PHENIX identified hadron yields [2] complemented with $K^*(892)/K^-$ and ϕ/K^- ratios measured by the STAR Collaboration [4, 5, 6].

However the possible expansion of the fireball is invisible in particle yield ratios (a collective flow is able to modify only the momentum spectra of a measured particle, but not its multiplicity). Therefore, in addition to the studies of particle ratios the analysis of the p_T spectra is necessary to gain some quantitative information about the flow. Such analysis was done for the chemical equilibrium case of the SHM (the third point of the list above) in Ref. [7]. In the present paper the similar analysis of the p_T spectra will be performed for both chemical non-equilibrium cases of the SHM (the first and the second point of the list above).

To describe the flow at the stage of the freeze-out, the single-freeze-out model of Refs. [8, 9, 10] is applied. The model succeeded in the accurate description of ratios and p_T spectra of particles measured at RHIC. The main postulate of

*Electronic address: prorok@ift.uni.wroc.pl

the model is the simultaneous occurrence of chemical and thermal freeze-outs, which means that the possible elastic interactions after the chemical freeze-out are neglected. The conditions for the freeze-out are expressed by values of two independent thermal parameters: T and μ_B. The second basic feature of the model is the complete treatment of resonance decays. This means that the final distribution of a given particle consists not only of the thermal part but also of contributions from all possible decays and cascades. Feeding from week decays is included as well. Since in the original formulation [8, 9, 10] this model corresponds to the chemical equilibrium case of the SHM, the generalization of the single-freeze-out model to chemical non-equilibrium cases of the SHM will be done in the present paper.

The global variables like the transverse energy at midrapidity ($dE_T/d\eta|_{mid}$), the charged particle multiplicity at midrapidity ($dN_{ch}/d\eta|_{mid}$) and the total multiplicity of charged particles (N_{ch}) are also evaluated for both chemical non-equilibrium cases of the SHM for different centrality bins of the PHENIX measurements at $\sqrt{s_{NN}} = 200$ GeV [11]. These three variables are independent observables, which means that they are measured independently of identified hadron spectroscopy. Since model fits were done to identified hadron data (particle yield ratios and p_T spectra) and the global variables are calculable in the generalized single freeze-out model, it was natural to check whether their estimated values agree with the data. This has proven to be true within 10% accuracy. It should be stressed also here that the centrality independence of the total multiplicity of charged particles per participant pair has been reproduced. The evidence for such scaling of the total multiplicity was reported by the PHOBOS Collaboration [12].

In some sense this work could be understood as an additional test of the correctness of the determination of the statistical parameters of the SHM since these parameters enter primordial distributions of hadrons in the fireball at the freeze-out. Thus fits of geometric parameters of the generalized single-freeze-out model are done with the use of the values of the statistical parameters obtained earlier in Ref. [1] and treated as input here. The general conclusion is that the best quality fits to the p_T spectra of identified hadrons are obtained for the strangeness chemical non-equilibrium case of the SHM. And what is surprising, in the chemical equilibrium case the spectra seem to be fitted better then in the scenario with the full chemical non-equilibrium. Whenever in this paper the term "strangeness chemical non-equilibrium case" or "full chemical non-equilibrium case" is used it means the case with its values of statistical parameters taken from Ref. [1] and listed in Table I, Sec. IV A. Additionally, the spectra of ϕ and $K(892)^{*0}$ resonances are predicted. In this way spectra of each particle species whose yield was used in determination of the statistical parameters of the model [1] are calculated in here. Also the measurement of the low momentum π^0 is proposed as a test, which could help to ascertain whether the full chemical non-equilibrium could happen in the fireball at the freeze-out or could not. Namely, values of γ_q determined in Ref. [1] cause that the predictions for low-p_T π^0 are about 40% greater in this case then in semi-equilibrium or equilibrium cases.

II. THE SINGLE-FREEZE-OUT MODEL AND ITS GENERALIZATION

The main assumptions of the model are as follows: (a) the chemical and thermal freeze-outs take place simultaneously, (b) all confirmed resonances up to a mass of 2 GeV from the Particle Data Tables [13] are taken into account, (c) a freeze-out hypersurface is defined by the equation

$$\tau = \sqrt{t^2 - r_x^2 - r_y^2 - r_z^2} = const \ , \tag{1}$$

(d) the four-velocity of an element of the freeze-out hypersurface is proportional to its coordinate

$$u^\mu = \frac{x^\mu}{\tau} = \frac{t}{\tau} \ \left(1, \frac{r_x}{t}, \frac{r_y}{t}, \frac{r_z}{t}\right) \ , \tag{2}$$

(e) the following parameterization of the hypersurface is chosen:

$$t = \tau \cosh\alpha_\parallel \cosh\alpha_\perp, \quad r_x = \tau \sinh\alpha_\perp \cos\phi, \quad r_y = \tau \sinh\alpha_\perp \sin\phi, \quad r_z = \tau \sinh\alpha_\parallel \cosh\alpha_\perp, \tag{3}$$

where $\alpha_\parallel$ is the rapidity of the element, $\alpha_\parallel = \tanh^{-1}(r_z/t)$, and $\alpha_\perp$ controls the transverse radius:

$$\rho = \sqrt{r_x^2 + r_y^2} = \tau \sinh\alpha_\perp < \rho_{max} \ , \tag{4}$$

where the restriction on the transverse size has been introduced, so ρ_{max} gives the maximal transverse extension of the gas in the central slice during the freeze-out. This means that two new parameters of the model have been introduced, *i.e.* τ and ρ_{max}, which are connected with the geometry of the freeze-out hypersurface.

From Eq. (1) one can see that the beginning of the freeze-out process starts at $t^{(1)}_{f.o.} = \tau$ and $\vec{r} = 0$ in the c.m.s., which is also the laboratory frame in the RHIC case. At this moment the volume of the gas can be estimated as

$$V^{(1)}_{f.o.} = 2\pi\tau\rho^2_{max} \, , \tag{5}$$

which is simply the volume of a tube with a length 2τ and a radius ρ_{max} (2τ is the maximal possible extension of the gas in the longitudinal direction at $t^{(1)}_{f.o.}$). In the central slice the freeze-out ceases at $t^{(2)}_{f.o.} = \sqrt{\tau^2 + \rho^2_{max}}$ and it takes place at $\rho = \rho_{max}$.

The transverse velocity in the central slice can be expressed as a function of the transverse radius

$$\beta_\perp(\rho) = \tanh\alpha_\perp = \frac{\rho}{\sqrt{\tau^2 + \rho^2}} \, . \tag{6}$$

The maximum value of $\beta_\perp$ called the maximum transverse-flow parameter (or the surface velocity) is given by

$$\beta^{max}_\perp = \frac{\rho_{max}}{\sqrt{\tau^2 + \rho^2_{max}}} = \frac{\rho_{max}/\tau}{\sqrt{1 + (\rho_{max}/\tau)^2}} \, . \tag{7}$$

The invariant distribution of the measured particles of species i has the form [8, 9]

$$\frac{dN_i}{d^2p_T \, dy} = \int p^\mu d\sigma_\mu \, f_i(p \cdot u) \, , \tag{8}$$

where $d\sigma_\mu$ is the normal vector on a freeze-out hypersurface, $p \cdot u = p^\mu u_\mu$, u_μ is the four-velocity of a fluid element and f_i is the final momentum distribution of the particle in question. The final distribution means here that f_i is the sum of primordial and simple and sequential decay contributions to the particle distribution (for details see [10, 14]).

For the most general case of the chemical non-equilibrium the primordial momentum distribution of particle species i is given by

$$f^{primordial}_i = \frac{(2s_i + 1)}{(2\pi\hbar c)^3} \, \frac{1}{\gamma_i^{-1} \exp\left\{\frac{E_i - \mu_i}{T}\right\} + g_i} \, , \tag{9}$$

where $E_i = (m_i^2 + p^2)^{1/2}$ and m_i, μ_i, s_i and g_i are the mass, chemical potential, spin and a statistical factor of species i respectively. The chemical potential $\mu_i = B_i\mu_B + S_i\mu_S + I^i_3\mu_{I_3}$, where B_i, S_i and I^i_3 are the baryon number, strangeness and the third component of the isospin of the particle species in question, whereas μ's are the corresponding overall chemical potentials. The strangeness chemical potential μ_S is determined from the requirement that the overall strangeness equals zero. The chemical potential related to the third component of the isospin, μ_{I_3}, is derived from the constraint that the charge to the net baryon ratio in the final state is the same as in the colliding nuclei. It has turned out that μ_{I_3} is negligible at RHIC ($\mid \mu_{I_3} \mid \leq 1$ MeV [1, 10]), so it will be omitted in further considerations. The non-equilibrium factor γ_i reads

$$\gamma_i = \gamma_q^{(N^i_q + N^i_{\bar{q}})} \gamma_s^{(N^i_s + N^i_{\bar{s}})} \, , \tag{10}$$

where $\gamma_{q(s)}$ is the light (strange) quark phase space occupancy factor, N^i_q and N^i_s are the numbers of light and strange quarks in the ith hadron, and $N^i_{\bar{q}}$ and $N^i_{\bar{s}}$ are the numbers of the corresponding antiquarks in the same hadron.

With the use of Eqs. (2) and (3), the invariant distribution (8) takes the following form:

$$\frac{dN_i}{d^2p_T \, dy} = \int d\sigma \, (p \cdot u) \, f_i(p \cdot u) = \tau^3 \int\limits_{-\infty}^{+\infty} d\alpha_\parallel \int\limits_0^{\rho_{max}/\tau} \sinh\alpha_\perp d(\sinh\alpha_\perp) \int\limits_0^{2\pi} d\xi \, (p \cdot u) \, f_i(p \cdot u) \, , \tag{11}$$

where

$$p \cdot u = m_T \cosh(\alpha_\parallel - y) \cosh\alpha_\perp - p_T \cos\xi \sinh\alpha_\perp \, . \tag{12}$$

III. TRANSVERSE ENERGY AND CHARGED PARTICLE MULTIPLICITY

The experimentally measured transverse energy is defined as

$$E_T = \sum_{i=1}^{L} \hat{E}_i \cdot \sin\theta_i \ , \tag{13}$$

where θ_i is the polar angle, $\hat{E}_i$ denotes $E_i - m_N$ (m_N means the nucleon mass) for baryons, $E_i + m_N$ for antibaryons and the total energy E_i for all other particles, and the sum is taken over all L emitted particles [11].

The pseudorapidity density of particle species i is given by

$$\frac{dN_i}{d\eta} = \int d^2p_T \ \frac{dy}{d\eta} \ \frac{dN_i}{d^2p_T \ dy} = \int d^2p_T \ \frac{p}{E_i} \ \frac{dN_i}{d^2p_T \ dy} \ . \tag{14}$$

Analogously, the transverse energy pseudorapidity density for the same species can be written as

$$\frac{dE_{T,i}}{d\eta} = \int d^2p_T \ \hat{E}_i \cdot \frac{p_T}{p} \ \frac{dy}{d\eta} \ \frac{dN_i}{d^2p_T \ dy} = \int d^2p_T \ p_T \ \frac{\hat{E}_i}{E_i} \ \frac{dN_i}{d^2p_T \ dy} \ . \tag{15}$$

For the quantities at midrapidity one has (in the c.m.s., which is the RHIC case)

$$\frac{dN_i}{d\eta} \Big|_{mid} = \int d^2p_T \ \frac{p_T}{m_T} \ \frac{dN_i}{d^2p_T \ dy} \ , \tag{16}$$

$$\frac{dE_{T,i}}{d\eta} \Big|_{mid} = \begin{cases} \int d^2p_T \ p_T \ \frac{m_T - m_N}{m_T} \ \frac{dN_i}{d^2p_T \ dy} \ , i = baryon \\ \int d^2p_T \ p_T \ \frac{m_T + m_N}{m_T} \ \frac{dN_i}{d^2p_T \ dy} \ , i = antibaryon \\ \int d^2p_T \ p_T \ \frac{dN_i}{d^2p_T \ dy} , i = others \ . \end{cases} \tag{17}$$

The overall charged particle and transverse energy densities can be expressed as

$$\frac{dN_{ch}}{d\eta} \Big|_{mid} = \sum_{i \in B} \frac{dN_i}{d\eta} \Big|_{mid} \ , \tag{18}$$

$$\frac{dE_T}{d\eta} \Big|_{mid} = \sum_{i \in A} \frac{dE_{T,i}}{d\eta} \Big|_{mid} \ , \tag{19}$$

where A and B ($B \subset A$) denote sets of species of finally detected particles, namely the set of charged particles $B = \{\pi^+, \ \pi^-, \ K^+, \ K^-, \ p, \ \bar{p}\}$, whereas A also includes photons, K^0_L, n and $\bar{n}$ [15].

The total multiplicity of particle species i can be also derived (for the more formal proof see [10])

$$\begin{aligned} N_i \ &= \ \int d^2p_T \ dy \ \frac{dN_i}{d^2p_T \ dy} = \int d^2p_T \ dy \int p^\mu d\sigma_\mu \ f_i(p \cdot u) = \int d\sigma \int d^2p_T \ dy \ (p \cdot u) \ f_i(p \cdot u) \\ &= \int d\sigma \int \frac{d^3\vec{p}}{E} \ (p \cdot u) \ f_i(p \cdot u) = \int d\sigma \ n_i(T, \mu_B, \gamma_s, \gamma_q) = n_i(T, \mu_B, \gamma_s, \gamma_q) \int d\sigma \ , \end{aligned} \tag{20}$$

for any expansion satisfying the condition $d\sigma_\mu \sim u_\mu$ on a freeze-out hypersurface and if the local statistical parameters are constant on this hypersurface (in the present model both conditions are fulfilled). Note that the density of particle species i, n_i, includes thermal and decay contributions. In practise the rapidity of the fluid element $\alpha_\parallel$ should not be unlimited but should have its maximal value $\alpha_\parallel^{max}$. Otherwise, the hypersurface volume and the total charged particle multiplicity would be infinite. Then one can express the hypersurface volume as

$$\int d\sigma = \tau^3 \int\limits_{-\alpha_\parallel^{max}}^{+\alpha_\parallel^{max}} d\alpha_\parallel \int\limits_0^{\rho_{max}/\tau} \sinh\alpha_\perp \; d(\sinh\alpha_\perp) \int\limits_0^{2\pi} d\xi = 2\pi \; \alpha_\parallel^{max} \tau \rho_{max}^2 \; . \tag{21}$$

Finally, the total multiplicity of charged particles can be obtained:

$$N_{ch} = 2\pi \; \alpha_\parallel^{max} \tau \rho_{max}^2 \sum_{i \in B} n_i(T, \mu_B, \gamma_s, \gamma_q) = 2\pi \; \alpha_\parallel^{max} \tau \rho_{max}^2 \; n_{ch}(T, \mu_B, \gamma_s, \gamma_q) \; . \tag{22}$$

For $\alpha_\parallel^{max}$ the following reasonable assumption has been made: it is equal to the rapidity of leading baryons after the collision. This means that the fluid which has been created in the central rapidity region (CRR) could not move faster in the longitudinal direction then fragments of a target or a projectile after the collision. Therefore $\alpha_\parallel^{max}$ should depend on the centrality of the collision, since the more central the collision is, the higher degree of the stopping of the initial baryons ought to happen in principle. There are two limiting cases, the maximum stopping happens for the most central collision whereas if the centrality approaches 100% the stopping disappears. Assuming additionally that $\alpha_\parallel^{max}$ is a linear function of the centrality, the following parametrization can be derived (for details see Ref. [7]):

$$\alpha_\parallel^{max}(c) = y_p - \frac{\langle \delta y \rangle}{0.975} \cdot (1 - c) \; , \tag{23}$$

where y_p is the projectile rapidity, $\langle \delta y \rangle$ the average rapidity loss and c is a fractional number representing the middle of a given centrality bin, *i.e.* $c = 0.025$ for the $0 - 5\%$ centrality bin, $c = 0.075$ for the $5 - 10\%$ centrality bin, etc.. The BRAHMS Collaboration reports $\langle \delta y \rangle = 2.05$ for the 5% most central collisions at $\sqrt{s_{NN}} = 200$ GeV ($y_p = 5.36$) [16].

IV. RESULTS

A. Determination of geometric parameters

The determination of parameters of the model proceeds in two steps. First, statistical parameters T, μ_B, γ_q and γ_s are fitted with the use of the experimental ratios of hadron multiplicities at midrapidity. This has been already done in Ref. [1] for all available centrality bins of the PHENIX measurements at $\sqrt{s_{NN}} = 200$ GeV [2]. Having put values of these parameters into the theoretical expression for the invariant distribution, Eqs. (11) and (12), two left parameters ρ_{max} and τ can be determined from the simultaneous fit to the transverse-momentum spectra of $\pi^\pm$, $K^\pm$, p and $\bar{p}$. The fits are performed with the help of the χ^2 method.

The final results for the geometric parameters ρ_{max} and τ are gathered in Table I together with the corresponding values of χ^2/NDF for each centrality class additionally characterized by the number of participants N_{part}. The results are given for all three cases of the SHM listed in Sec. I (for comparison the results for the chemical equilibrium case are repeated from Ref. [7]). Other physical quantities like the surface velocity $\beta_\perp^{max}$, the volume at the beginning of the freeze-out $V_{f.o.}^{(1)}$ and the maximal freeze-out time at the central slice $t_{f.o.}^{(2)}$ are also given there. Values of ρ_{max} and τ (therefore also $V_{f.o.}^{(1)}$ and $t_{f.o.}^{(2)}$) obtained in the case of full chemical non-equilibrium are substantially lower than corresponding values in the both other cases. This is because γ_s and γ_q are significantly greater than 1 in this case, so primordial densities given by Eqs. (9) and (10) are also greater than in both other cases. And since fits are done to the same spectra, to keep the normalization unchanged, values of the geometric parameters have to decrease.

Except the last three rows of Table I, all fits have been done with the use of the p_T spectra of identified charged hadrons measured by the PHENIX Collaboration in $\sqrt{s_{NN}} = 200$ GeV Au-Au collisions [2, 17]. Centrality classes with footnote marks denote two bins for which fitted spectra are taken from Ref. [17]. These are $0 - 10\%$ and $10 - 40\%$ centrality bins and they are not included in Ref. [2], so values of the statistical parameters have not been fitted for them in Ref. [1]. But for these bins ϕ meson spectra have been reported in Ref. [17]. Thus to make predictions for ϕ spectra, values of the statistical parameters have been taken as the averages of the values fitted for bins which added percent coverage equals $0 - 10\%$ or $10 - 40\%$. In the last three rows of Table I there are results of fits to the PHENIX data complemented with the low-p_T data for $\pi^\pm$ extracted from the PHOBOS measurements of $(\pi^+ + \pi^-)$ [18]. Since the particle ratio of $\pi^-/\pi^+ \approx 1$ independently of p_T and centrality (see e.g. Ref. [2]), the low-p_T values of π^+ and π^-

TABLE I: Values of the geometric parameters of the model for various centrality bins fitted with the use of the PHENIX final data for the p_T spectra of identified charged hadrons [2], NDF=124. For bins with footnotes a and b the data are from Ref. [17]. Values of the statistical parameters are taken from [1]. The last three rows show the results of fits to the set of data which include the PHENIX data and low-p_T π^+ and π^- data taken as a half of the PHOBOS data for $(\pi^+ + \pi^-)$ [18], here NDF=132.

Centrality [%]	N_{part}	T [MeV]	μ_B [MeV]	γ_s	γ_q	ρ_{max} [fm]	τ [fm]	$\beta_\perp^{max}$	$V_{f.o.}^{(1)}$ [fm^3]	$t_{f.o.}^{(2)}$ [fm]	χ^2/NDF
0-5	351.4	141.1	25.67	2.430	1.613	7.24±0.09	6.61±0.06	0.74	2177.5	9.8	0.74
5-10	299.0	141.4	24.52	2.367	1.61169	6.82±0.08	6.17±0.06	0.74	1804.4	9.2	0.73
0-10[a]	325.2	141.25	25.095	2.3985	1.6125	7.03±0.08	6.39±0.06	0.74	1985.8	9.5	0.80
10-15	253.9	141.6	25.27	2.270	1.603	6.46±0.08	5.81±0.06	0.74	1525.6	8.7	0.72
15-20	215.3	140.8	25.05	2.266	1.61497	6.16±0.08	5.48±0.05	0.75	1304.8	8.2	0.85
20-30	166.6	141.0	26.01	2.212	1.61387	5.58±0.07	4.96±0.05	0.75	969.7	7.5	1.24
30-40	114.2	142.0	25.75	2.096	1.608	4.76±0.07	4.33±0.05	0.74	617.0	6.4	1.64
10-40[b]	171.8	141.35	25.52	2.211	1.61	5.80±0.07	5.17±0.05	0.75	1093.7	7.8	1.28
40-50	74.4	141.7	26.14	2.003	1.605	4.06±0.06	3.80±0.04	0.73	392.6	5.6	2.02
50-60	45.5	141.0	24.05	1.876	1.613	3.39±0.06	3.32±0.04	0.71	239.1	4.7	1.96
60-70	25.7	140.2	25.32	1.636	1.618	2.72±0.05	2.86±0.04	0.69	133.0	3.9	2.16
70-80	13.4	141.7	24.24	1.026	1.299	2.40±0.06	2.78±0.05	0.65	100.6	3.7	1.43
0-5	351.4	154.6	25.04	1.231	1.0	8.35±0.10	8.57±0.08	0.70	3752.1	12.0	0.57
5-10	299.0	155.2	24.73	1.186	1.0	7.84±0.10	7.97±0.08	0.70	3077.1	11.2	0.43
0-10[a]	325.2	154.9	24.885	1.2085	1.0	8.10±0.09	8.27±0.07	0.70	3407.3	11.6	0.56
10-15	253.9	155.5	26.29	1.169	1.0	7.37±0.10	7.41±0.07	0.70	2527.0	10.4	0.36
15-20	215.3	154.6	25.68	1.147	1.0	7.07±0.10	7.04±0.07	0.71	2212.2	10.0	0.39
20-30	166.6	155.2	27.18	1.121	1.0	6.37±0.09	6.32±0.06	0.71	1609.9	9.0	0.53
30-40	114.2	155.7	27.21	1.080	1.0	5.47±0.08	5.51±0.06	0.70	1036.6	7.8	0.78
10-40[b]	171.8	155.25	26.59	1.1293	1.0	6.65±0.08	6.60±0.06	0.71	1833.5	9.4	0.53
40-50	74.4	155.5	26.74	1.018	1.0	4.65±0.07	4.82±0.06	0.69	654.6	6.7	1.07
50-60	45.5	152.6	21.62	0.8906	1.0	4.06±0.07	4.39±0.06	0.68	455.2	6.0	1.04
60-70	25.7	152.2	26.12	0.8076	1.0	3.22±0.07	3.73±0.05	0.65	243.0	4.9	1.32
70-80	13.4	148.6	23.82	0.7163	1.0	2.59±0.06	3.17±0.06	0.63	133.6	4.1	1.20
80-92	6.3	150.8	28.00	0.6788	1.0	1.92±0.06	2.69±0.06	0.58	62.3	3.3	1.21
0-5	351.4	155.2	26.4	1.0	1.0	8.46±0.10	8.84±0.08	0.69	3973.4	12.2	0.80
5-10	299.0	155.2	26.4	1.0	1.0	7.99±0.10	8.23±0.08	0.70	3302.6	11.5	0.61
0-10[a]	325.2	155.2	26.4	1.0	1.0	8.23±0.09	8.54±0.07	0.69	3629.8	11.9	0.80
10-15	253.9	155.2	26.4	1.0	1.0	7.54±0.10	7.67±0.08	0.70	2736.2	10.8	0.48
15-20	215.3	155.2	26.4	1.0	1.0	7.11±0.10	7.17±0.07	0.70	2275.5	10.1	0.48
20-30	166.6	155.2	26.4	1.0	1.0	6.45±0.09	6.47±0.07	0.71	1689.5	9.1	0.58
30-40	114.2	155.2	26.4	1.0	1.0	5.57±0.08	5.63±0.06	0.70	1097.2	7.9	0.77
10-40[b]	171.8	155.2	26.4	1.0	1.0	6.74±0.08	6.76±0.06	0.71	1932.3	9.6	0.64
40-50	74.4	155.2	26.4	1.0	1.0	4.68±0.07	4.85±0.06	0.69	669.0	6.7	1.05
50-60	45.5	155.2	26.4	1.0	1.0	3.83±0.07	4.16±0.05	0.68	383.9	5.7	1.13
60-70	25.7	155.2	26.4	1.0	1.0	2.99±0.06	3.47±0.05	0.65	194.3	4.6	1.41
70-80	13.4	155.2	26.4	1.0	1.0	2.22±0.06	2.78±0.05	0.62	86.3	3.6	1.55
80-92	6.3	155.2	26.4	1.0	1.0	1.71±0.06	2.40±0.05	0.58	44.2	2.9	1.40
0-15[c]	303.0	141.4	25.15	2.356	1.609	6.82±0.08	6.09±0.05	0.75	1778.0	9.1	0.87
0-15[c]	303.0	155.1	25.35	1.195	1.0	7.87±0.10	8.00±0.07	0.70	3111.7	11.2	0.41
0-15[c]	303.0	155.2	26.4	1.0	1.0	8.02±0.10	8.26±0.08	0.70	3337.0	11.5	0.59

[a]Here statistical parameters are the averages of the parameters listed in two sequential rows above this row.
[b]Here statistical parameters are the averages of the parameters listed in four sequential rows above this row.
[c]Here statistical parameters are the averages of the parameters given for the $0-5\%$, $5-10\%$ and $10-15\%$ centrality classes in the same case of the SHM.

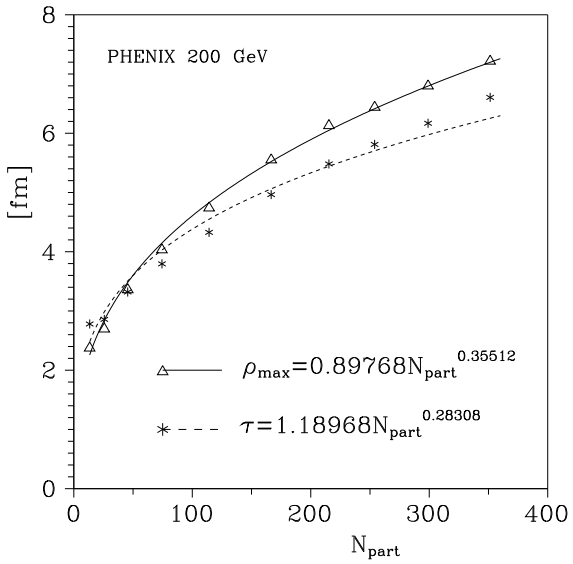

FIG. 1: Values of the geometric parameters of the model from the seventh and eighth column of Table I for for the full chemical non-equilibrium case ($\gamma_s \neq 1$, $\gamma_q \neq 1$). The lines are the best power approximations.

spectra have been taken as one half of $(\pi^+ + \pi^-)$ reported by PHOBOS. However, some modification of the original PHENIX data [2] has been done to match the PHOBOS data conditions. Namely, the PHOBOS measurements were done for the 15% most central collisions ($N_{part} = 303$), whereas the PHENIX ones for the $0-5\%$, $5-10\%$ and $10-15\%$ centrality bins. Since the treatment of counts includes the averaging over the number of events in a given centrality bin and for the same run the number of events in the 15% most central bin should be equal to the sum of numbers of events in the $0-5\%$, $5-10\%$ and $10-15\%$ centrality bins, the rough approximation of the hypothetic measurement done in the $0-15\%$ centrality bin would be the average of the measurements done in the $0-5\%$, $5-10\%$ and $10-15\%$ centrality bins. Such averages have been taken as the PHENIX data for the $0-15\%$ centrality bin. Also values of the statistical parameters taken for this case are the appropriate averages of the values given for the $0-5\%$, $5-10\%$ and $10-15\%$ centrality bins.

As it can be seen from the last column of Table I, the best quality fits have been obtained for the strangeness chemical non-equilibrium case of the SHM. Also fits done in the chemical equilibrium case are slightly better than those presented for the full chemical non-equilibrium. This conclusion can be expressed in an informal quantifiable way by calculating the average of χ^2/NDF for each case of the SHM. So, for the chemical full non-equilibrium $\langle\chi^2/\mathrm{NDF}\rangle = 1.30$, for the strangeness chemical non-equilibrium $\langle\chi^2/\mathrm{NDF}\rangle = 0.77$ and for the chemical equilibrium $\langle\chi^2/\mathrm{NDF}\rangle = 0.9$. Also the wider range of centrality fulfils the condition of the statistical significance, *i.e.* $\chi^2/\mathrm{NDF} < 1$, in the both cases of $\gamma_q = 1$ (up to 40% of centrality) than in the case of $\gamma_q \neq 1$ (up to 20% of centrality). Fits done with the inclusion of the low-p_T $\pi^{\pm}$ measured by PHOBOS have confirmed the above conclusion, as it can be seen in three last rows of Table I.

Values of the geometric parameters ρ_{max} and τ from Table I are presented in Figs. 1-2 as functions of N_{part}. Also there the lines of the best power approximations are depicted,

$$x \sim N_{part}^{\kappa}, \qquad x = \rho_{max},\ \tau, \tag{24}$$

with a scaling exponent $\kappa \approx 0.36$ for ρ_{max} and $\kappa \approx 0.28$ for τ.

B. Identified hadron spectra

Having obtained parameters of the model the spectra can be given with the use of Eqs. (11) and (12). In Figs. 3 and 4 (top plots) the spectra of sums of negative and positive identified hadrons are depicted. This way of presentation is chosen to confront the model predictions for low-p_T values of spectra with the PHOBOS experimental data [18]. Since the PHOBOS data are for the $0-15\%$ centrality bin, the PHENIX data for this bin have been simulated in the same way as explained in Sec. IV A.

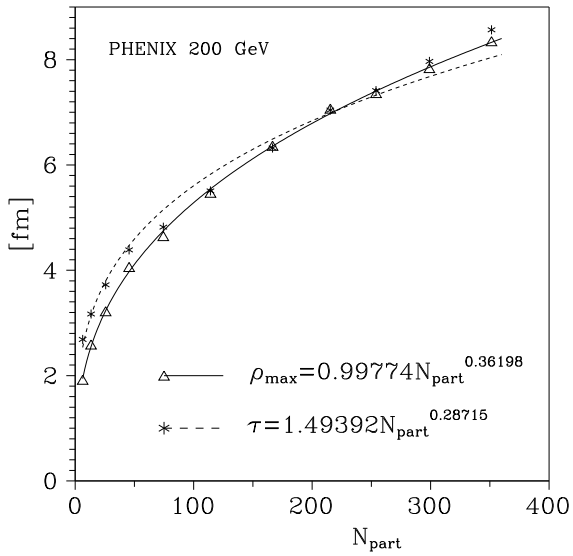

FIG. 2: Values of the geometric parameters of the model from the seventh and eighth column of Table I for the strangeness chemical non-equilibrium case ($\gamma_s \neq 1$, $\gamma_q = 1$). The lines are the best power approximations.

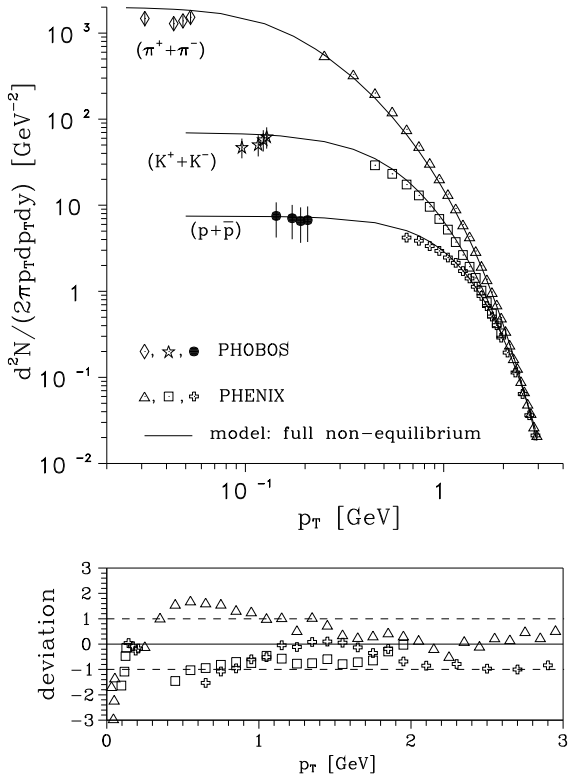

FIG. 3: The top plot presents invariant yields as a function of p_T for RHIC at $\sqrt{s_{NN}} = 200$ GeV. The PHOBOS data are for the 15% most central collisions with the error bars expressed as the sum of the systematic and statistical uncertainties [18]. The corresponding PHENIX data [2] are presented as the averages of the invariant yields for $0-5\%$, $5-10\%$ and $10-15\%$ centrality bins. For the PHENIX data errors are about 10% and are of the size of symbols. Lines are the appropriate predictions of the single-freeze-out model for the full chemical non-equilibrium case (fit to the PHENIX data only). The bottom plot shows a deviation of data to the model, $(f_{exp} - f_{theo})/\sigma_{exp}$, where $f_{exp(theo)}$ is the experimental (theoretical) value of the invariant yield at given p_T and σ_{exp} is the error of f_{exp}. Both PHENIX and PHOBOS data are denoted by the same symbol for the same species, *i.e.* triangles are for $(\pi^+ + \pi^-)$, squares for $(K^+ + K^-)$ and open crosses for $(p + \bar{p})$.

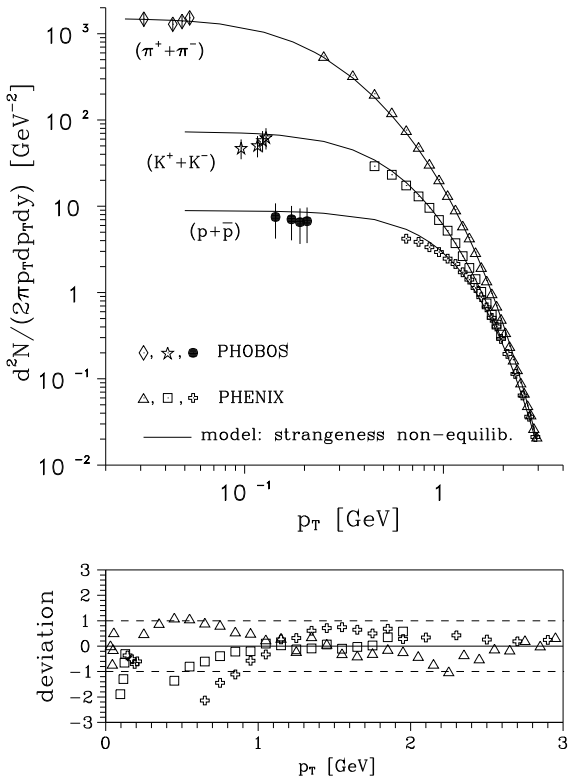

FIG. 4: Same as Fig. 3 but for the strangeness chemical non-equilibrium case.

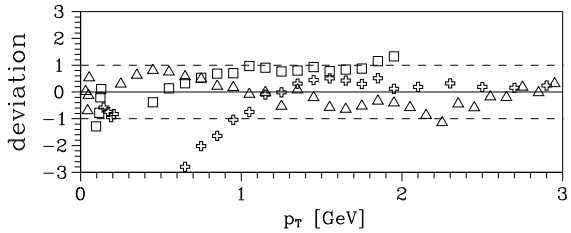

FIG. 5: Same as the bottom plot of Fig. 3 but for the chemical equilibrium case.

In the case of chemical full non-equilibrium, Fig. 3, the low-p_T pions are mostly overestimated ($\approx 33\%$), after then kaons ($\approx 21\%$) and the best predictions have been made for protons and antiprotons ($\approx 5\%$ above the data). In the case of chemical strangeness non-equilibrium, Fig. 4, it is opposite, pions are predicted exactly, but kaons and protons and antiprotons are overestimated roughly equally ($\approx 25\%$). For the chemical equilibrium case (see Fig. 4 in Ref. [7], it looks almost the same as the top plot of Fig. 4 here) the situation in the low-p_T range is similar to this in the chemical strangeness non-equilibrium case, namely pions are in complete agreement with the data, kaons are $\approx 13\%$ above and protons and antiprotons are the most overestimated, $\approx 34\%$. The above discussion confirms the conclusion drawn from the comparison of the values of χ^2/NDF - the chemical strangeness non-equilibrium case seems to work in the best way as far as fits to the spectra are considered.

To visualize the quality of fits and overall predictions, in the bottom plots of Figs. 3 and 4 and in Fig. 5 deviations of data to the model are presented. The deviation is defined as

$$\frac{f_{exp} - f_{theo}}{\sigma_{exp}} \,, \tag{25}$$

where $f_{exp(theo)}$ is the experimental (theoretical) value of the invariant yield at given p_T and σ_{exp} is the error of f_{exp}. The number of points which are entirely outside of the ± 1 band is the greatest in the case of chemical full non-equilibrium (21, the most of them corresponds to pions with all the low-p_T sample counted). In the both other

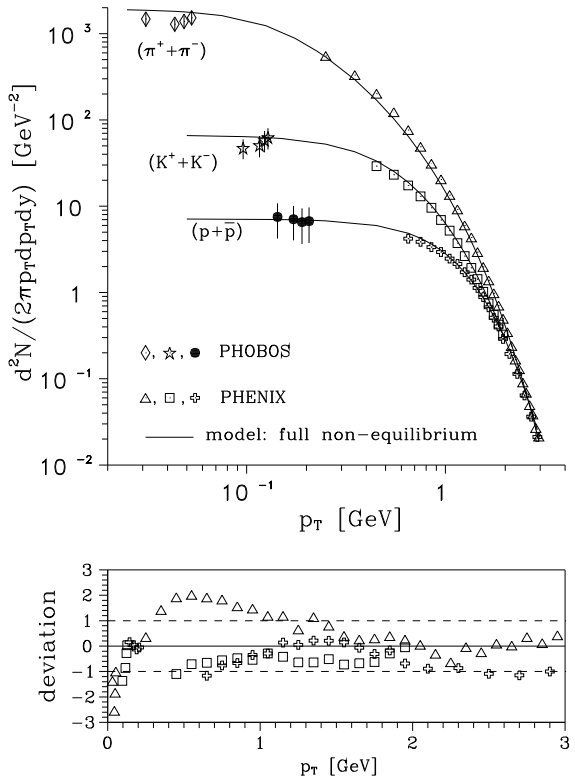

FIG. 6: Same as Fig. 3 but for the simultaneous fit to the PHENIX and low-p_T $\pi^{\pm}$ PHOBOS data.

cases this number is the same and equals 8. Also the widest deviation is in the first case, it reaches -2.9, whereas in the case of chemical strangeness non-equilibrium the farthest point is -2.1 and in the chemical equilibrium case -2.8.

To investigate into this problem from the other side, fits for the 15% most central bin have been done with the inclusion of the low-p_T $\pi^{\pm}$ taken from the PHOBOS data [18]. The data give values of $(h^+ + h^-)$ spectra of identified hadrons ($h = \pi,\ K,\ p$) at very low p_T. But only for pions the particle ratio of $h^-/h^+ \approx 1$ independently of p_T and centrality at RHIC (see e.g. Ref. [2]). Thus values of $\pi^{\pm}$ spectra for very low p_T are taken as one half of $(\pi^+ + \pi^-)$ reported by PHOBOS [18]. The results of fits have been gathered in the last three rows of Table I. The corresponding spectra are presented in the top plots of Figs. 6-8. In the bottom plots of Figs. 6-8 deviations of data to the model are depicted. Deviation figures shows explicitly what is expressed by the values of χ^2/NDF given in Table I - in the chemical strangeness non-equilibrium case spectra are fitted much better then in both other cases. The number of points outside the ± 1 band equals 9 in this case and the farthest one is at -2.1 (see the bottom plot of Fig. 7). In the chemical full non-equilibrium case this number is 19 and the farthest point is at -2.5 (see the bottom plot of Fig. 6). In the chemical equilibrium case the number of points outside the ± 1 band is 8, but one of them reaches the value -2.8 (see the bottom plot of Fig. 8).

From what has been explained so far one can see that the chemical full non-equilibrium freeze-out seems to be less likely in comparison with semi-equilibrium and equilibrium cases. And if $\gamma_q = 1$ indeed, both last cases will be practically undistinguishable, however semi-equilibrium will be in favor.

C. ϕ and $K(892)^{*0}$ spectra

In this subsection the predictions for the spectra of ϕ and $K(892)^{*0}$ resonances will be discussed. This is an interesting point since the yields of these resonances measured by the STAR Collaboration [4, 5, 6] were used (with the basic yields of the identified hadrons measured by the PHENIX Collaboration [2]) to fit the statistical parameters of the model [1]. In the fitting procedure presented here (to obtain the geometric parameters of the model ρ_{max} and τ, see Sec. IV A), identified hadron spectra measured by PHENIX [2] have been explored. So the main source of the data used to test the SHM here and in Ref. [1] is the PHENIX measurement at $\sqrt{s_{NN}} = 200$ GeV. But predictions of the model should be compared with both PHENIX and STAR data, since the STAR data on $K^*(892)/K^-$ and ϕ/K^- ratios were also used in fits of the statistical parameters in Ref. [1]. However, one should keep in mind, when

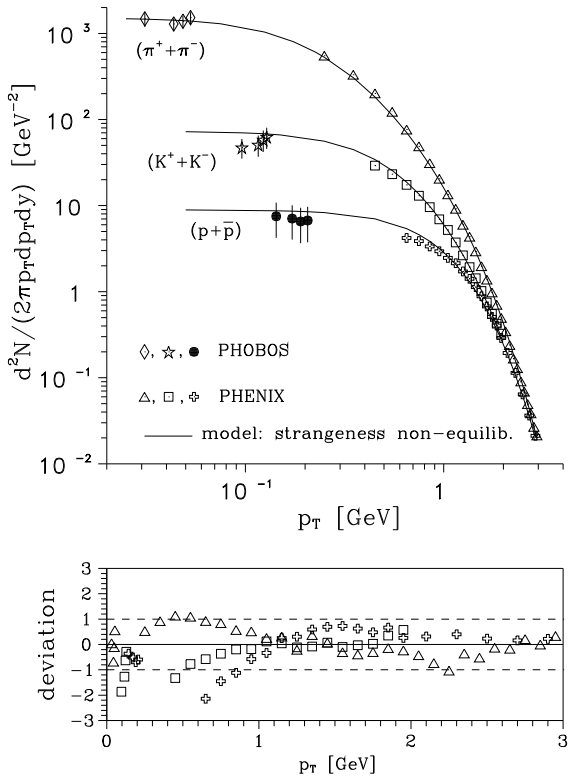

FIG. 7: Same as Fig. 4 but for the simultaneous fit to the PHENIX and low-p_T $\pi^{\pm}$ PHOBOS data.

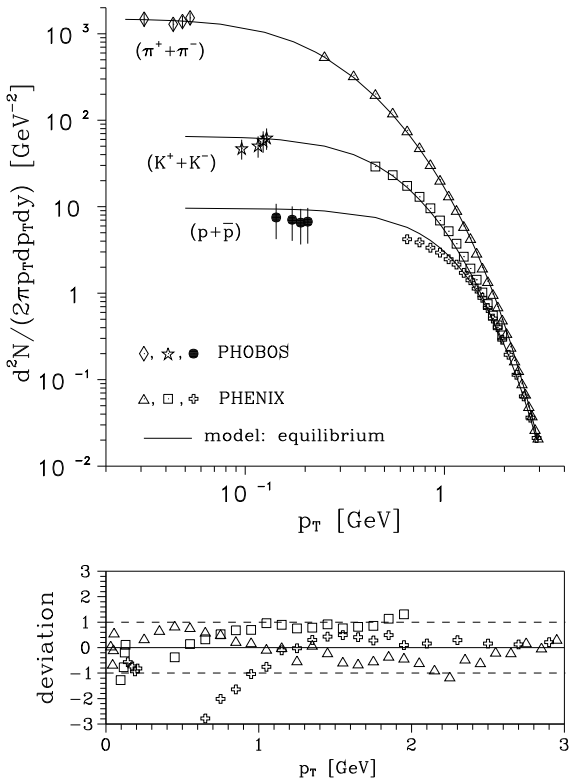

FIG. 8: Same as Fig. 7 but for the chemical equilibrium case.

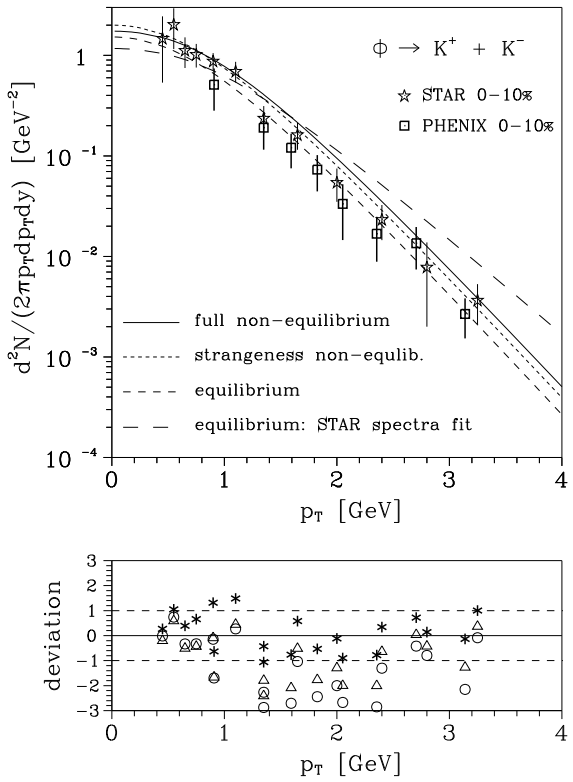

FIG. 9: The top plot presents invariant yields of ϕ meson measured via the K^+K^- decay channel as a function of p_T for the $0-10\%$ centrality bin at $\sqrt{s_{NN}} = 200$ GeV. Data are from Refs. [6] (STAR) and [17] (PHENIX). The bottom plot shows a deviation of the data to the model predictions based on fits to the PHENIX spectra: chemical full non-equlibrium (circles), strangeness non-equilibrium (triangles) and chemical equilibrium (asterisks).

the ϕ spectra are discussed, that the $\approx 70\%$ difference has been found between ϕ yields at midrapidity measured by STAR [6] and PHENIX [17] for one common centrality been, $0-10\%$. The reason for such behavior is still unknown and this is probably not a statistical fluctuation of the lowest m_T PHENIX point, as suggested in Ref. [1], because when the same m_T range for both the STAR and the PHENIX ϕ data is considered the difference still persists (see Ref. [59] in Ref. [17]).

In Figs. 9 and 10 predictions for the ϕ production are presented for $0-10\%$ and $10-40\%$ centrality classes of the PHENIX measurement for all three cases of the SHM analyzed here. Additionally, the results for the equilibrium case but such that the statistical and geometric parameters of the model are fitted to the STAR data only are also depicted. This is the case considered in Ref. [7]: the statistical parameters ($T = 160.0$ MeV, $\mu_B = 24.0$ MeV) are fitted to the STAR particle yield ratios [19] and the geometric parameters to the p_T spectra of identified hadrons delivered by the STAR Collaboration in Ref. [20]. Again, since the STAR identified hadron spectra [20] are for different centrality classes than the STAR ϕ-spectra [6], the values of geometric parameters for $0-10\%$ and $10-30\%$ centrality bins explored by STAR in ϕ meson measurements are the averages of the values fitted in Ref. [7] for bins which added percent coverage equals $0-10\%$ and $10-30\%$ respectively. This gives $\rho_{max} = 8.81$ fm, $\tau = 6.98$ fm for the $0-10\%$ centrality bin and $\rho_{max} = 7.035$ fm, $\tau = 6.095$ fm for the $10-30\%$ centrality bin. Results corresponding to these two equilibrium (STAR) cases are presented as long-dashed lines in Figs. 9 and 10. Also both the PHENIX and the STAR data are depicted in these figures. Note that the STAR second bin is $10-30\%$, whereas the second PHENIX bin is $10-40\%$ (see Fig. 10). Generally, as one can see in Figs. 9 and 10, all three cases of the SHM agree qualitatively with both the PHENIX and the STAR data when the predictions are based on the fits to the PHENIX spectra (solid, short-dashed and dashed lines). When the predictions are based on the fit to the STAR spectra (long-dashed lines) they agree with the STAR data only up to the intermediate transverse momentum range and overestimate the high p_T data. It is not clear why this happens, but within the PHENIX experiment the picture is consistent.

Since Figs. 9 and 10 are in the logarithmic scale, to see quantitative agreement or disagreement of each SHM case, one should go somehow to the linear scale. This has been done in the bottom plots of Figs. 9 and 10, where deviations of both the PHENIX and the STAR data to the model are depicted for all three cases of the SHM considered here. It is clearly seen that predictions in the equilibrium case are substantially better than in the both non-equilibrium

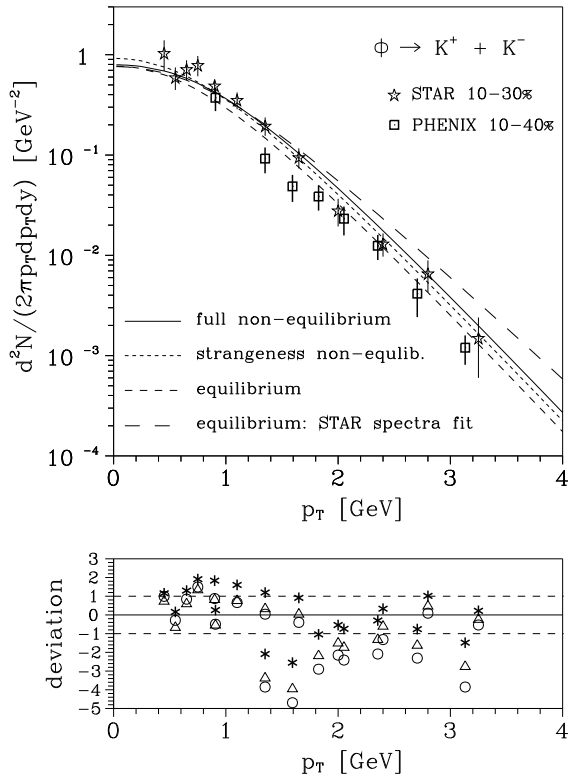

FIG. 10: Same as Fig. 9 but for the $10-40\%$ centrality bin. Note that STAR data are for the $10-30\%$ centrality bin.

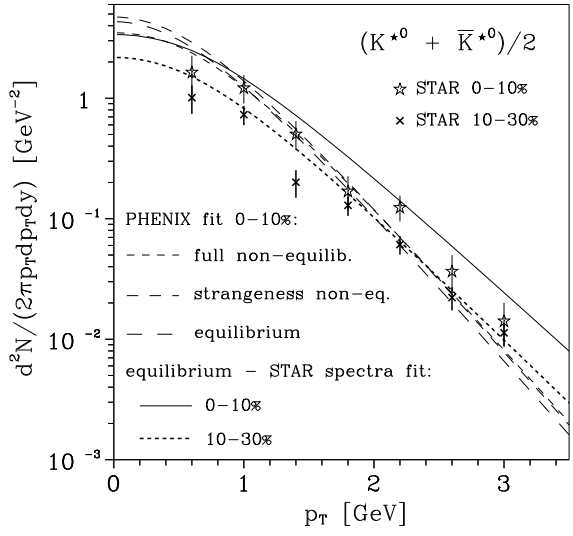

FIG. 11: The invariant yields of $(K^{*0} + \bar{K}^{*0})/2$ as a function of p_T for $0-10\%$ and $10-30\%$ centrality bins at $\sqrt{s_{NN}} = 200$ GeV. Data are from Ref. [5]

cases. In fact, the both non-equilibrium cases are practically ruled out, however the strangeness non-equilibrium case seems to behave slightly better than the full non-equilibrium case.

In Fig. 11 results for $(K^{*0} + \bar{K}^{*0})/2$ spectra are presented together with the STAR data for $0-10\%$ and $10-30\%$ centrality classes [5]. This figure is very instructive since it explicitly shows that the data from different collaborations should not be mixed in any fitting procedure. As one can see predictions based on fitting to the PHENIX data for the $0-10\%$ centrality class (*cf.* Table I) are very similar to each other and miss the STAR data on the $(K^{*0} + \bar{K}^{*0})/2$ production mainly because of the different slope. In fact, these predictions are above the level of the STAR data for

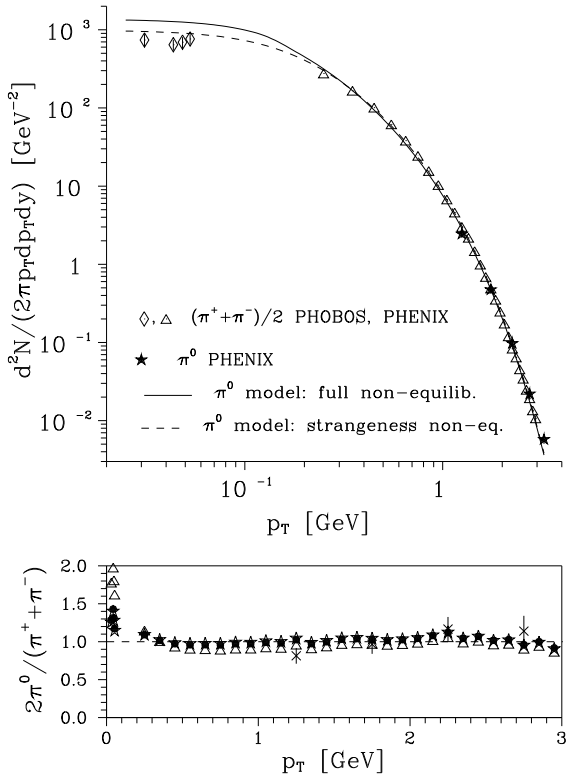

FIG. 12: The top plot presents invariant yields of π^0 in comparison with the half of $(\pi^+ + \pi^-)$ yields for RHIC at $\sqrt{s_{NN}} = 200$ GeV. The PHOBOS data (diamonds) are for the 15% most central collisions [18]. The corresponding PHENIX data [2] (triangles) are presented as the averages of the invariant yields for the $0-5\%$, $5-10\%$ and $10-15\%$ centrality bins. The PHENIX data for π^0 (stars) are for the 10% most central bin [21]. For both PHENIX data errors are about 10% and are of the size of symbols. Lines are the appropriate predictions of the single-freeze-out model. The bottom plot shows a ratio of predicted π^0 to the half of measured $(\pi^+ + \pi^-)$ for the full chemical non-equilibrium case (triangles), the strangeness chemical non-equilibrium case (dots) and the chemical equilibrium case (open stars). Also values of the ratio calculated with the use of the experimental data are depicted (crosses).

the $0-10\%$ centrality class in the low transverse momenta but they are below even the STAR data for the $10-30\%$ centrality class in the high transverse momenta. Additionally, the results for the equilibrium case but such that the statistical and geometric parameters of the model are fitted to the STAR data only are also depicted. This is the case considered in Ref. [7]: the statistical parameters ($T = 160.0$ MeV, $\mu_B = 24.0$ MeV) are fitted to the STAR particle yield ratios [19] and the geometric parameters to the p_T spectra of identified hadrons delivered by the STAR Collaboration in Ref. [20]. Again, since the STAR identified hadron spectra [20] are for different centrality classes than the STAR $(K^{*0} + \bar{K}^{*0})/2$ spectra [5], the values of geometric parameters for $0-10\%$ and $10-30\%$ centrality bins explored by STAR in $(K^{*0} + \bar{K}^{*0})/2$ measurements are the averages of the values fitted in Ref. [7] for bins which added percent coverage equals $0-10\%$ and $10-30\%$ respectively. This gives $\rho_{max} = 8.81$ fm, $\tau = 6.98$ fm for the $0-10\%$ centrality bin and $\rho_{max} = 7.035$ fm, $\tau = 6.095$ fm for the $10-30\%$ centrality bin. Results corresponding to these two equilibrium (STAR) cases are presented as solid and shortest-dashed lines in Figs. 11. In fact some overestimation in normalization can be seen, mostly in the case of the $0-10\%$ centrality bin, but slopes are correct.

D. π^0 spectra

The occupancy factor γ_q, when differs from one, could influence the π^0 spectra strongly. This is because for π^0 $N_q = N_{\bar{q}} = 1$ and $N_s = N_{\bar{s}} = 0$. Then in the primordial distribution of π^0 one has (see Eq. (9))

$$\gamma_{\pi^0}^{-1} \exp\left\{\frac{E_{\pi^0}}{T}\right\} = \exp\left\{\frac{E_{\pi^0} - \mu_\pi}{T}\right\} , \tag{26}$$

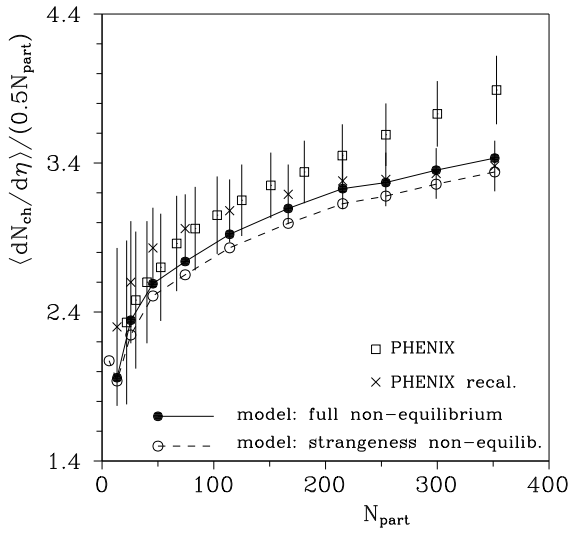

FIG. 13: $dN_{ch}/d\eta$ per pair of participants versus N_{part} for RHIC at $\sqrt{s_{NN}} = 200$ GeV. The original PHENIX data are from Ref. [11], whereas the recalculated PHENIX data are from summing up the integrated charged hadron yields delivered in Ref. [2]. The lines connect the results and are a guide.

where the chemical potential of pions is defined as

$$\mu_\pi = 2T \ln \gamma_q \ . \tag{27}$$

It has turned out that in the case of chemical full non-equilibrium

$$\mu_\pi \approx m_{\pi^0} \quad (\text{but} \ \ \mu_\pi \leq m_{\pi^0} \ \ \text{always}) \tag{28}$$

for the fitted values of γ_q and T taken from Ref. [1] and listed in Table I. This means that in this case the values of the statistical parameters happen to hit the critical values for the Bose-Einstein condensation of neutral pions. This has been already stated by the authors of Ref. [1] in Refs. [22, 23], namely that if γ_q is freed from 1 but is kept in the range $[1, \gamma_q^{cr} = e^{m_{\pi^0}/2T}]$, it goes to its critical value γ_q^{cr} during fitting procedure. If this happened really, this could enhance the production of π^0's with very low p_T.

Predictions for π^0 spectra are presented in Fig. 12 for two non-equilibrium cases of the SHM. The π^0 spectrum in the chemical equilibrium case is roughly the same as that for the chemical strangeness non-equilibrium case, so it is not depicted. However it is impossible to compare the predictions for the low p_T with the data since the appropriate data have not been available yet. Thus in Fig. 12 the comparison is done with the half of $(\pi^+ + \pi^-)$ spectrum delivered by PHOBOS for the 15% most central bin [18] and with the corresponding spectrum compiled from the PHENIX data [2]. As it is shown in the bottom plot of Fig. 12, the experimental ratio of $2\pi^0/(\pi^+ + \pi^-) \approx 1$ in the range of p_T common for $\pi^\pm$ [2] and π^0 [21] PHENIX measurements at $\sqrt{s_{NN}} = 200$ GeV, *i.e.* for $1 < p_T < 3$ GeV.

One can see from the top plot of Fig. 12 that down to the $p_T \approx 0.2$ GeV all three cases of the SHM predict roughly the same spectrum of π^0 (the curve for the chemical equilibrium case is not depicted because, in the logarithmic scale, it would exactly cover the curve for the chemical strangeness non-equilibrium case). The difference between predictions in the chemical full non-equilibrium case and predictions in both other cases arises at very low transverse momenta and is about 40%. This can be seen very clearly in the bottom plot of Fig. 12, where the ratio of predicted π^0 to the half of measured $(\pi^+ + \pi^-)$ is depicted as a function of p_T for all three cases of the SHM. The enhancement of neutral pions over one half of charged pions is $\approx 80\%$ in the case of chemical full non-equilibrium, whereas for both other cases is $\approx 30\%$. This suggests that the measurement of very low p_T π^0's could be helpful to judge whether $\gamma_q \approx \gamma_q^{cr}$ (as is claimed in Refs. [1, 22, 23] on the basis of fits to particle yields/ratios) or $\gamma_q = 1$.

E. Transverse energy and charged particle multiplicity estimations

The results of numerical estimations of $dN_{ch}/d\eta|_{mid}$ divided by the number of participant pairs for various centrality classes are presented in Fig. 13 for RHIC at $\sqrt{s_{NN}} = 200$ GeV. The results are given for two non-equilibrium cases of

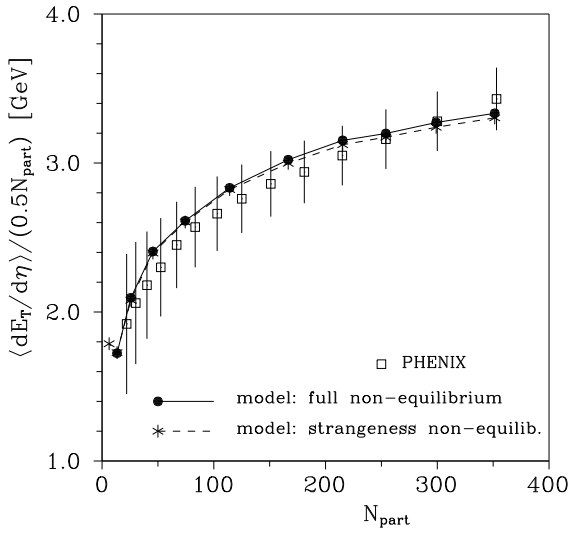

FIG. 14: $dE_T/d\eta$ per pair of participants versus N_{part} for RHIC at $\sqrt{s_{NN}} = 200$ GeV. The PHENIX data are from Ref. [11]. The lines connect the results and are a guide.

the SHM (the estimates in the case of chemical equilibrium are almost the same as in the chemical strangeness non-equilibrium case and have been already presented in Ref. [7], see Fig.6 therein). Additionally to the straightforward PHENIX measurements of the charged particle multiplicity density, the data from the summing up of the integrated charged hadron yields [2] are depicted in these figures, too (these data are called "recalculated", for more explanations see Ref. [7]). Note that the recalculated data differ from the direct ones, especially for more central bins. This has been already noticed by the PHENIX Collaboration (see backup slides of [24]). In [2] the feeding of $p(\bar{p})$ from $\Lambda(\bar{\Lambda})$ decays is excluded. To diminish this effect, integrated p and $\bar{p}$ yields delivered in [2] were corrected to include back the feeding. The correction was done by the division by a factor 0.65, which is the rough average of a p_T-dependent multiplier used by PHENIX Collaboration (see Fig.4 in [2] and Eq.(5) therein).

Generally, in both presented cases the model predictions underestimate the directly measured (more) as well as recalculated (less) $dN_{ch}/d\eta|_{mid}$. However, the estimates in the chemical full non-equilibrium case are slightly closer to the data and for the four most central bins they agree entirely with the recalculated data points. In the full range of centrality the predictions agree with the recalculated data within errors in this case and almost agree within errors in the chemical strangeness non-equilibrium case. In principle, since the fits of the geometric parameters of the model have been done to the same p_T spectra here, which were integrated to deliver charged hadron yields in Ref. [2], the predictions for $dN_{ch}/d\eta|_{mid}$ should agree exactly with the recalculated data. However, the transverse momentum spectra are measured in *limited ranges*, so very important low-p_T regions are blank in Ref. [2]. To obtain integrated yields some extrapolations below and above the measured ranges are used. In fact these extrapolations are only analytical fits, but contributions from regions covered by them account for about $25-40\%$ of the integrated yields [25]. These extrapolations could differ from the distributions obtained in the framework of this model and this could be the main source of the discrepancy between the predictions and the recalculated data. So the question why the significant underestimation of the predicted $dN_{ch}/d\eta|_{mid}$ with respect to the directly measured charged particle multiplicity density occurs should be addressed to the experimentalists rather: why does the directly measured $dN_{ch}/d\eta|_{mid}$ differ substantially from the sum of the integrated hadron yields for central collisions?

The values of $dE_T/d\eta|_{mid}$ per pair of participants as a function of participant pairs are shown in Fig. 14 for $\sqrt{s_{NN}} = 200$ GeV. The quality of the model predictions is much better in this case then for $dN_{ch}/d\eta|_{mid}$, they agree with the data almost completely. Note that predictions in both presented cases are practically the same and do not differ from the corresponding results in the chemical equilibrium case (see Fig.7 in Ref. [7]).

Values of the ratio $\langle dE_T/d\eta\rangle/\langle dN_{ch}/d\eta\rangle$ as a function of N_{part} are presented in Fig. 15. Again, as for $dN_{ch}/d\eta|_{mid}$, the values predicted in the chemical full non-equilibrium case are slightly closer to the data, they agree with the recalculated data within errors. For the most central bins both sets of predictions agree with the recalculated data within errors. $\langle dE_T/d\eta\rangle/\langle dN_{ch}/d\eta\rangle$ estimates done within the chemical equilibrium case are practically the same as in the strangeness non-equilibrium case (see Fig.10 in Ref. [7]). As far as the comparison with the direct data [11] is concerned, the position of model predictions is very regular and exactly resembles the configuration of the data in each case, the estimates are only shifted up about 10% as a whole.

The last discussed global variable is the total multiplicity of charged particles N_{ch}, which can be calculated with

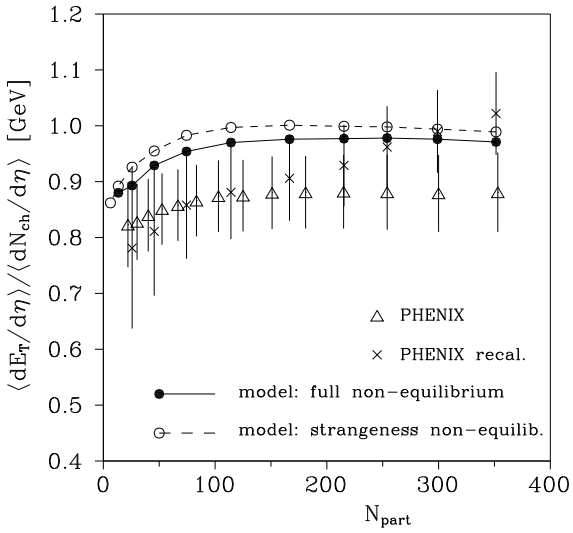

FIG. 15: $\langle dE_T/d\eta\rangle/\langle dN_{ch}/d\eta\rangle$ versus N_{part} for RHIC at $\sqrt{s_{NN}} = 200$ GeV. The original PHENIX data are from Ref. [11]. The recalculated PHENIX data are also depicted, here "recalculated" means that the sum of integrated charged hadron yields [2] have been substituted for the denominator in the ratio. The lines connects the results and are a guide.

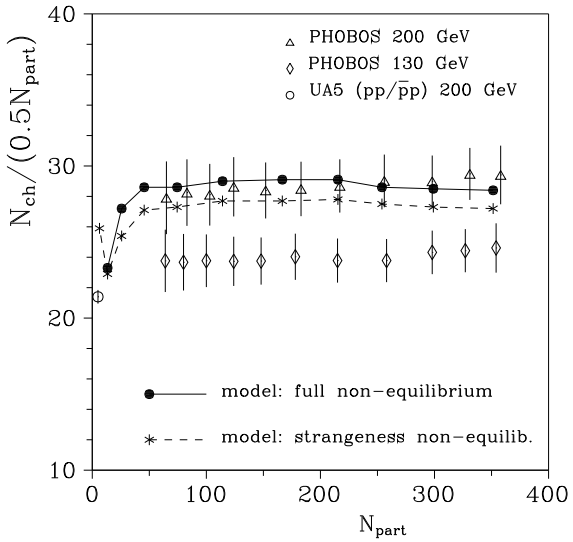

FIG. 16: N_{ch} per pair of participants versus N_{part} for RHIC at $\sqrt{s_{NN}} = 200$ GeV. The PHOBOS data are from Ref. [12] and the $pp/\bar{p}p$ data point of the UA5 measurement is from Fig.39.5 in Ref. [13]. The lines connect the results and are a guide.

the use of Eqs. (22) and (23). The results presented as the total charged-particle multiplicity per participating pair versus N_{part} are gathered in Fig. 16. The both sets of predictions exhibit almost ideal centrality independence within the range of the PHOBOS measurement, *i.e.* $N_{part} \approx 60 - 360$. Note that in the chemical full non-equilibrium case also normalization agrees almost exactly with the data. In the case of chemical strangeness non-equilibrium the 6% underestimation has resulted but the predictions still agree with the data within errors. For the chemical equilibrium the similar underestimation was obtained (6.4%, see Fig.12 in Ref. [7]).

The general conclusion which could be drawn from the above discussion is that predictions for global variables agree pretty well with the data in each case of the SHM. However, the chemical full non-equilibrium scenario works slightly better in this respect.

V. CONCLUSIONS

The extensive analysis of the RHIC data on the particle production in Au-Au collisions at $\sqrt{s_{NN}} = 200$ GeV has been performed within three possible scenarios of the statistical hadronization model. The SHM explored here is the generalized version of the model of Ref. [1]. The generalization means the explicite inclusion of the fireball expansion in a way as proposed in the single-freeze-out model of Refs. [8, 9, 10].

Generally no definite rejection of any of these scenarios could be done on the basis of this analysis, since different observables prefer different scenarios. However, the chemical full non-equilibrium case seems to be the least likely. This is evident from the studies of particle spectra of stable charged hadrons, both from the statistical significance point of view (values of χ^2/NDF in Table I) and from the behavior of the deviation factor (bottom plots of Figs. 3-8). The ϕ-spectrum test confirms the above conclusion (see Sec. IV C). On the opposite, the global variable test prefers the full chemical non-equilibrium scenario and does not distinguish between strangeness chemical non-equilibrium and chemical equilibrium cases (see Sec. IV E) but the differences are not significant. The semi-equilibrium and equilibrium scenarios seem to be of the similar likelihood, even though the ϕ-spectrum analysis discredits the strangeness chemical non-equilibrium case. This is because the fits to spectra of identified charged hadrons seem to weigh most when the conclusion is to be drawn from the present studies. The p_T spectra of stable charged hadrons comprise the most numerous and of the highest quality samples of the experimental data. For each centrality class of the PHENIX measurement at $\sqrt{s_{NN}} = 200$ GeV, the p_T spectra counts more than 120 points, whereas each sample of the discussed resonance spectra or of the global variable has about 10 points. Also the measurement of a stable charged hadron seems to be more accurate since such a hadron is measured directly while resonances can be measured only via their decay products. The last point which supports the relevance of the fits to identified hadron spectra is that all data used in the fitting procedure (here particle yields and p_T spectra) and the data which predictions are compared with, should originate from the same experiment, as it has been shown explicitly in Sec. IV C in the example of $(K^{*0} + \bar{K}^{*0})/2$ spectra (Fig. 11). This is the case of the fits to identified hadron spectra, since the statistical parameters were fitted to the sample comprising 6 particle yields from PHENIX ($\pi^{\pm}$, $K^{\pm}$, p and $\bar{p}$) and only 2 yield ratios from STAR (see Ref. [1]). And with these parameters entering the expression for the invariant distribution, Eq. (11), p_T spectra of $\pi^{\pm}$, $K^{\pm}$, p and $\bar{p}$ measured by PHENIX have been fitted to determine the geometric parameters of the model. Thus the main results presented in Table I have been obtained within practically one experiment, *i.e.* the PHENIX Collaboration.

The above remark should be kept in mind when the SHM predictions for yields of other particles (other then used in the fitting procedure) are compared with the data. For instance, in Ref. [26] predictions for (anti)hyperons were done on the basis of fits from Ref. [1] (that is fits done to the data set of which the main part is from PHENIX at $\sqrt{s_{NN}} = 200$ GeV). However the conclusion is drawn from the comparison with the STAR data at $\sqrt{s_{NN}} = 130$ GeV. The conclusion is that the chemical full non-equilibrium case is in favor. But in the main figure of Ref. [26] (Fig.2 there), which has led to this conclusion, there are no corresponding predictions in the strangeness chemical non-equilibrium case. It is only stated there that these predictions are in between the chemical full non-equilibrium and the chemical equilibrium cases. All above arguments suggest that the strangeness chemical non-equilibrium case as well as the chemical equilibrium case have not been discredited entirely in the context of the (anti)hyperon production.

Also particle yield fluctuations has been proposed as a definite test of what scenario of the SHM is the most likely [27] but one has to await for the appropriate data to make a conclusion. This test distinguishes between (semi)equilibrium and non-equilibrium scenarios. But what is interesting, values of the statistical parameters given there for the chemical full non-equilibrium case are again at the condition for the Bose-Einstein condensation of neutral pions, $\gamma_q \approx \gamma_q^{cr}$, (these values are $T = 140.0$ MeV and $\gamma_q = 1.62$ [27], which gives $\mu_\pi = 135.079$ MeV, Eq. (27), so $\mu_\pi > m_{\pi^0}$ but this is the matter of rounding off [28], if one takes $\gamma_q = 1.619$ then $\mu_\pi < m_{\pi^0}$). In fact, as it is explained in Refs. [22, 23], γ_q^{cr} is the upper limit of the allowed range of γ_q superimposed before the fitting procedure has started. So by definition $\gamma_q \leq \gamma_q^{cr}$ always (if the value of γ_q put in a table of Refs. [1, 22, 23] happens to exceed γ_q^{cr} this is the result of rounding up [28], as in the above-mentioned example). But from the technical point of view, when γ_q slightly exceeds this limit the fitting procedure will still proceed, since π^0 yield is not included in the set of yields and/or ratios to fit. So the true upper limit should be $e^{m_{\pi^\pm}/2T}$ rather, because exceeding this limit causes divergences in primordial densities of π^+ and π^-, yields of which are included usually in the set of data to fit. Thus the fitted values of γ_q [1, 22, 23] seem to be not trustworthy. All these facts put in question the idea of introducing the parameter γ_q into the model. But this supports the conclusion that the chemical full non-equilibrium freeze-out is the least likely. Anyway, if values of γ_q were at the critical point for the Bose-Einstein condensation of π^0 (as it is claimed in Refs. [1, 22, 23]), then the significant π^0-overproduction at low-p_T could happen with respect to one half of $(\pi^+ + \pi^-)$ (see Sec. IV D), which seems to be checkable at least in principle.

And the last remark is that the present analysis has been done within a particular hypersurface, as given by Eqs. (1)-(4). Of course, the natural question is to what extend the results depend on the choice of a hypersurface. One of the

indirect arguments pro this hypersurface are the results of fits to the PHENIX spectra of $\pi^{\pm}$, $K^{\pm}$, p and $\bar{p}$ done in Ref. [17] within the very popular blast-wave model [29]. For those fits $\chi^2/\mathrm{NDF} \approx 3-4$, so from the statistical point of view such a hypothesis should be rejected. On the opposite, in the present work $\chi^2/\mathrm{NDF} < 1$ has been obtained for all central and mid-central bins (see Table I). Thus at least for these bins the hypothesis that the hypersurface has the form as given here can not be rejected. Also the discussed possible overproduction of low-p_T π^0's seems not to depend very much on a form of the hypersurface chosen since this effect is the result of approaching the condition for the Bose-Einstein condensation of neutral pions. This causes the abrupt increase of the distribution function of π^0, $f_{\pi^0}^{primordial}(p \cdot u)$, when $p_T \to 0$ for all hypersurfaces which have a region with the negligible flow.

To summarize, in the view of this analysis the chemical full non-equilibrium freeze-out seems to happen least likely during Au-Au collisions at $\sqrt{s_{NN}} = 200$ GeV and both other cases are of the similar likelihood. To help to verify this conclusion, the low-p_T π^0 measurement is proposed since at low p_T the ratio of π^0 over one half of $(\pi^+ + \pi^-)$ distinguishes very clearly between $\gamma_q \approx \gamma_q^{cr}$ and $\gamma_q = 1$.

Acknowledgments

The author would like to thank Jan Rafelski and Wojciech Florkowski for very helpful discussions. This work was supported in part by the Polish Committee for Scientific Research under Contract No. KBN 2 P03B 069 25.

[1] J. Rafelski, J. Letessier and G. Torrieri, Phys. Rev. C **72**, 024905 (2005).
[2] S. S. Adler *et al.* [PHENIX Collaboration], Phys. Rev. C **69**, 034909 (2004).
[3] J. Letessier and J. Rafelski, Cambridge Monogr. Part. Phys. Nucl. Phys. Cosmol. **18** 1 (2002).
[4] H. B. Zhang [STAR Collaboration], arXiv:nucl-ex/0403010.
[5] J. Adams *et al.* [STAR Collaboration], Phys. Rev. C **71**, 064902 (2005).
[6] J. Adams *et al.* [STAR Collaboration], Phys. Lett. B **612**, 181 (2005).
[7] D. Prorok, Phys. Rev. C **73**, 064901 (2006).
[8] W. Broniowski and W. Florkowski, Phys. Rev. Lett. **87**, 272302 (2001).
[9] W. Broniowski and W. Florkowski, Phys. Rev. C **65**, 064905 (2002).
[10] W. Broniowski, A. Baran and W. Florkowski, Acta Phys. Polon. B **33**, 4235 (2002).
[11] S. S. Adler *et al.* [PHENIX Collaboration], Phys. Rev. C **71**, 034908 (2005) [Erratum-ibid. C **71**, 049901 (2005)].
[12] B. B. Back *et al.* [PHOBOS Collaboration], Phys. Rev. C **74**, 021902(R) (2006).
[13] K. Hagiwara *et al.* [Particle Data Group Collaboration], Phys. Rev. D **66**, 010001 (2002).
[14] D. Prorok, Eur. Phys. J. A **24**, 93 (2005).
[15] K. Adcox *et al.* [PHENIX Collaboration], Phys. Rev. Lett. **87**, 052301 (2001).
[16] I. G. Bearden *et al.* [BRAHMS Collaboration], Phys. Rev. Lett. **93**, 102301 (2004).
[17] S. S. Adler *et al.* [PHENIX Collaboration], Phys. Rev. C **72**, 014903 (2005).
[18] B. B. Back *et al.* [PHOBOS Collaboration], Phys. Rev. C **70**, 051901(R) (2004).
[19] O. Barannikova [STAR Collaboration], J. Phys. G **31**, S93 (2005).
[20] J. Adams *et al.* [STAR Collaboration], Phys. Rev. Lett. **92**, 112301 (2004).
[21] S. S. Adler *et al.* [PHENIX Collaboration], Phys. Rev. Lett. **91**, 072301 (2003).
[22] J. Rafelski and J. Letessier, Acta Phys. Polon. B **34**, 5791 (2003).
[23] J. Letessier and J. Rafelski, arXiv:nucl-th/0504028.
[24] T. Chujo [PHENIX Collaboration], Nucl. Phys. A **715**, 151 (2003) and `http://alice-france.in2p3.fr/qm2002/Transparencies/20Plenary/Chujo.ppt`.
[25] K. Adcox *et al.* [PHENIX Collaboration], Phys. Rev. Lett. **88**, 242301 (2002).
[26] J. Letessier and J. Rafelski, Phys. Rev. C **73**, 014902 (2006).
[27] G. Torrieri, S. Jeon and J. Rafelski, Phys. Rev. C **74**, 024901 (2006).
[28] J. Rafelski (private communication).
[29] E. Schnedermann, J. Sollfrank and U. Heinz, Phys. Rev. C **48**, 2462 (1993).